Journal of Coordination Chemistry

ISSN: 0095-8972 (Print) 1029-0389 (Online) Journal homepage: http://www.tandfonline.com/loi/gcoo20

Asymmetric N_2O_2 complexes of iron(III) and nickel(II) obtained from acetylacetone-S-methyl-thiosemicarbazone: synthesis, characterization and electrochemistry

Büşra Kaya, Atif Koca & Bahri Ülküseven

To cite this article: Büşra Kaya, Atif Koca & Bahri Ülküseven (2015) Asymmetric N_2O_2 complexes of iron(III) and nickel(II) obtained from acetylacetone-S-methyl-thiosemicarbazone: synthesis, characterization and electrochemistry, Journal of Coordination Chemistry, 68:4, 586-598, DOI: 10.1080/00958972.2014.989843

To link to this article: http://dx.doi.org/10.1080/00958972.2014.989843

Accepted author version posted online: 19 Nov 2014.
Published online: 15 Dec 2014.

Journal of Coordination Chemistry, 2015
Vol. 68, No. 4, 586–598, http://dx.doi.org/10.1080/00958972.2014.989843

Asymmetric N_2O_2 complexes of iron(III) and nickel(II) obtained from acetylacetone-S-methyl-thiosemicarbazone: synthesis, characterization and electrochemistry

BÜŞRA KAYA†, ATIF KOCA‡ and BAHRI ÜLKÜSEVEN*†

†Department of Chemistry, Istanbul University, Istanbul, Turkey
‡Engineering Faculty, Chemical Engineering Department, Marmara University, Istanbul, Turkey

(*Received 18 August 2014; accepted 30 October 2014*)

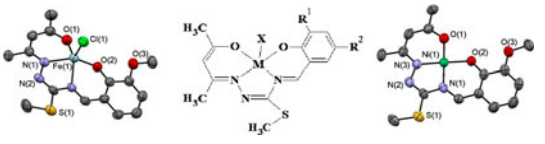

R^1, R^2 are H, Br, Cl or OCH_3

Iron(III) and nickel(II) complexes from acetylacetone-S-methyl-thiosemicarbazone were synthesized and characterized. The thiosemicarbazidato structures of N_2O_2 are N^1-acetylacetone, N^4-salicyl/3-methoxy/5-bromo-/3,5-dichlorosalicylidene. The square-pyramidal iron(III) and square-planar nickel (II) complexes of N^1-acetylacetone-N^4-3-methoxy thiosemicarbazidato were determined by X-ray diffraction. Electrochemical characterizations of the complexes were carried out by using cyclic voltammetry and square wave voltammetry. While nickel(II) complexes only give ligand based reduction and oxidation reactions, iron(III) complexes give reversible Fe^{III}/Fe^{II} reduction in addition to the ligand based processes. Changing of the substituents on the ligand, shifts the redox processes and also affects the stabilities of the electrogenerated species. With respect to the reduction potential of Fe^{III}/Fe^{II} couple, the most easily reduced complex was 3,5-dichloro substituted complexes and the most difficult to reduce was the 3-methoxy substituted one.

Keywords: Thiosemicarbazone; Iron(III); Nickel(II); Structural analysis; Electrochemistry

1. Introduction

Thiosemicarbazones are multidentate ligands, having a wide range of biological activities depending on the parent carbonyl compounds [1, 2]. Transition metal complexes of thiosemicarbazones also show various biological activities such as antitumor [3–5], antimicrobial [6–8], antiviral [9–11], antioxidant [12], and cytotoxic [13, 14] effects.

Numerous metal complexes with some N_4, N_3O, or N_2O_2 chelating 2-hydroxy-arylidene-thiosemicarbazones have been reported [15–17]. Characterization of the N_3O and N_2O_2

*Corresponding author. Email: bahseven@istanbul.edu.tr

complexes derived from acetylacetone thiosemicarbazones have been limited. One is a copper(II) complex with an N_3O chelating benzoylacetone thiosemicarbazone [18], and, only a few N_2O_2 complexes with copper(II) and nickel(II) have obtained thiosemicarbazones of acetylacetone and benzoylacetone [19–21].

Iron(III) and nickel(II) complexes of N_2O_2-type thiosemicarbazidato ligands have cytotoxic activity on K562 leukemia cell lines [14, 22], and thus, studies related to this class of thiosemicarbazones are noteworthy for improving chemotherapy agents.

Herein, we present the first iron(III) complexes in the type of N_2O_2 from acetylacetone-S-methyl-thiosemicarbazone as the starting material, and also four new nickel(II) complexes of the same ligand were synthesized. The N^1-acetylacetone, N^4-salicyl/3-methoxy/5-bromo, and 3,5-dichloro salicylidene-thiosemicarbazidato structures in **1–8** were characterized by elemental analysis, IR, ^{1}H-NMR, and mass spectra (figure 1). Structural confirmation of the N_2O_2 chelates was carried out by X-ray diffraction analysis of the iron(III) and nickel(II) complexes (**3** and **7**) bearing the 3-methoxy substituent.

To understand the influences on biological systems, the redox properties of the complexes were determined to illustrate the effect of the substituents to the electrochemical behaviors and to predict their possible use in different electrochemical technologies.

2. Experimental

2.1. *Materials and physical measurements*

All chemicals were reagent grade and used as purchased. Analytical data were obtained with a Thermo Finnigan Flash EA 1112 analyzer. UV–visible spectra were obtained in 10^{-5} M $CHCl_3$ solution using an ATI-Unicam UV/visible spectrometer. IR spectra of the compounds were recorded on KBr pellets with a Mattson 1000 FT-IR spectrometer. ^{1}H-NMR spectra were recorded on a Varian UNITY INOVA-500 MHz spectrometer relative to $SiMe_4$ using deuterated solvents. The APCI-MS analysis was carried out in positive and negative ion modes using a Thermo Finnigan LCQ Advantage MAX LC/MS/MS.

Single crystals of **3** and **7** for X-ray diffraction analyses were obtained by slow evaporation of alcohol solutions at room temperature. In **3**, $C_{15}H_{17}ClFeN_3O_3S$, having approximate dimensions of 0.60 × 0.40 × 0.05 mm and black crystal of **7**, $C_{15}H_{17}N_3NiO_3S$, having approximate dimensions of 0.80 × 0.40 × 0.10 mm were mounted on a glass fiber. The data were collected at room temperature to maximum 2θ values of 50.1° for **3** and 50.5° for **7**.

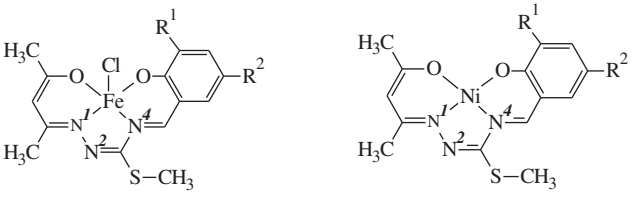

Figure 1. R^1, R^2 are H, H; H, Br; OCH_3, H; Cl, Cl for iron(III) (**1–4**) and nickel(II) (**5–8**) complexes, respectively.

All measurements were made on a Rikagu R-Axis Rapid-S imaging plate area detector with monochromated Mo-Kα radiation (λ = 0.71070 Å). The data were corrected for Lorentz and polarization effects and the structures of **3** and **7** were solved by direct methods by using the program SIR92 [23]. Hydrogen atoms were refined using the riding model and the non-hydrogen atoms were refined anisotropically. All calculations were performed using the Crystal Structure crystallographic software package [24, 25].

Electrochemical and spectroelectrochemical measurements were carried out with a Gamry Reference 600 potentiostat/galvanostat utilizing a three-electrode configuration at 25 °C. For cyclic voltammetry (CV), controlled potential coulometry (CPC), and square wave voltammetry (SWV) measurements, the working electrode was a Pt disk with a surface area of 0.071 cm^2. The surface of the working electrode was polished with a diamond suspension before each run. A Pt wire served as the counter electrode. A saturated calomel electrode was employed as the reference electrode and separated from the bulk of the solution by a double bridge. Ferrocene was used as an internal reference. Tetrabutylammonium perchlorate (TBAP) in DMSO and dichloromethane (DCM) was used. Nitrogen was used to remove dissolved O_2 at least 15 min prior to each run and to maintain a nitrogen blanket during the measurements. IR compensation was applied to the CV and SWV scans to minimize the potential control error.

2.2. *Synthesis*

Acetylacetone-S-methyl-thiosemicarbazone was obtained by literature method [26, 27]. The cream crystals melt at 169–170 °C. Anal. Calcd for $C_7H_{13}N_3OS$ (187.26): C, 44.90; H, 7.00; N, 22.44; S, 17.12. Found (%): C, 44.87; H, 6.98; N, 22.40; S, 16.95. UV–vis: 240 (4.4), 255 (4.4), 358 (3.8). IR: $\nu_{as}(NH_2)$ 3327, $\nu_s(NH_2)$ 3260, $\delta(NH_2)$, $\nu(C{=}N^1)$, $\nu(N^2{=}C)$ 1637–1539, ν(C–S) 738. ^{1}H NMR: 9.39, 8.95 (*cis*/*trans* ratio: 1/3, s, 2H, NH_2), 7.70 (s, 1H, O*H*), 3.73 (s, 2H, –CH_2–), 2.59 (s, 3H, S–CH_3), 2.08 (s, 3H, C–CH_3), 1.73 (s, 3H, C–CH_3).

For synthesis of the iron(III) complex (**1**), $FeCl_3{\cdot}6H_2O$ (0.27 g, 1 mM) was dissolved in methanol (5 mL) and then 1.5 mL of orthoformic ester was added to the solution. After letting it stand for 24 h at room temperature, a solution of the thiosemicarbazone (0.19 g, 1 mM) and 2-hydroxybenzaldehyde (0.1 mL, 1 mM) in 5 mL methanol was added dropwise to the metal salt solution. After addition of triethylamine (0.1 mM), the mixture was left to stand at room temperature overnight. The resulting precipitate is in the form of black powder. The solid product was filtered and recrystallized from ethanol. The other iron(III) and nickel(II) chelates (**2–8**) were prepared by a similar procedure.

The color, m.p. (°C), yields (%), elemental analysis, characteristic UV–vis [λ_{max} (log ε), nm ($dm^3\ cm^{-1}\ M^{-1}$)], and characteristic IR (cm^{-1}) bands, and NMR (500 MHz, $CDCl_3$, ppm) data of **1–8** were given as follows:

1: Black, 350, 40. Anal. Calcd for $C_{14}H_{15}N_3O_2SFeCl$ (380.65 g/M): C, 44.17; H, 3.97; N, 11.04; S, 8.42. Found (%): C, 43.96; H, 4.01; N, 10.82; S, 7.86. UV–vis: 240 (4.8), 290 (4.9), 421 (4.5), 536 (3.7). IR: $\nu(C{=}N^1)$ 1619, $\nu(N^2{=}C)$ 1585 $\nu(N^4{=}C)$ 1573.

2: Black, 210, 40. Anal. Calcd for $C_{14}H_{14}N_3O_2SFeClBr$ (459.54 g/M): C, 36.59; H, 3.07; N, 9.14; S, 6.98. Found (%): C, 36.55; H, 3.01; N, 9.01; S, 7.04. UV–vis: 235 (4.9), 285 (5.0), 421 (4.5), 529 (3.8). IR: $\nu(C{=}N^1)$ 1610, $\nu(N^2{=}C)$ 1593, $\nu(N^4{=}C)$ 1577.

3: Black, 266, 30. Anal. Calcd for $C_{15}H_{17}N_3O_3SFeCl$ (410.67 g/M): C, 43.87; H, 4.17; N, 10.23; S, 7.81. Found (%): C, 43.86; H, 4.24; N, 10.02; S, 6.99. UV–vis: 240 (4.7), 298

(4.9), 429 (4.4), 551 (3.5). IR: ν(C=N^1) 1607, ν(N^2=C) 1585, ν(N^4=C) 1571. *m/z* (+c ESI-MS): 375.2 ($M^+ - Cl$, 100%), 376.0 ([M − Cl + H], 22%).

4: Black, 269, 35. Anal. Calcd for $C_{14}H_{13}N_3O_2SFeCl_3$ (449.54 g/M): C, 37.40; H, 2.91; N, 9.35; S, 7.13. Found (%): C, 37.42; H, 3.17; N, 9.20; S, 7.00. UV–vis: 240 (4.8), 290 (4.9), 418 (4.5), 569 (3.5). IR: ν(C=N^1) 1612, ν(N^2=C) 1594, ν(N^4=C) 1576. *m/z* (+c ESI-MS): 448.8 ($[M-1]^+$, 100%), 450.0 ([M + 1], 36%), 415.8 ([M − Cl + H], 57%), 402.4 ([M − (SCH_3)], 52%).

5: Claret red, 209–210, 60. Anal. Calcd for $C_{14}H_{15}N_3O_2SNi$ (348.04 g/M): C, 48.31; H, 4.34; N, 12.07; S, 9.21. Found (%): C, 48.26; H, 4.38; N, 11.96; S, 9.02. UV–vis: 240 (4.7), 288 (4.4), 356 (4.2), 404.5 (4.1), 474 (4.0), 546 (3.6). IR: ν(C=N^1) 1623, ν(N^2=C) 1606, ν(N^4=C) 1581. ^{1}H NMR: 7.85 (s, 1H, N^4=C*H*), 7.32 (d, J = 7.33, 1H, *d*), 7.29 (d, J = 1.95, 1H, *b*), 7.13 (d, J = 9.27, 1H, *a*), 6.63 (ddd, J = 7.33, J = 8.29, 1H, *c*), 5.19 (s, 1H,=C*H*), 2.59 (s, 3H, S–CH_3), 2.15 (s, 3H, C–CH_3), 2.11 (s, 3H, C–CH_3).

6: Claret red, 280, 35. Anal. Calcd for $C_{14}H_{14}N_3O_2SNiBr$ (426.94 g/M): C, 39.38; H, 3.31; N, 9.84; S, 7.51. Found (%): C, 39.12; H, 3.21; N, 9.23; S, 7.23. UV–vis: 240 (4.7), 290 (4.3), 359 (4.2), 412 (4.1), 486 (4.0), 564 (3.5). IR: ν(C=N^1) 1607, ν(N^2=C) 1585, ν(N^4=C) 1575. ^{1}H NMR: 7.79 (s, 1H, N^4=C*H*), 7.47 (d, J = 2.44, 1H, *d*), 7.29–7.34 (m, 1H, *b*), 7.05 (d, J = 9.28, 1H, *a*), 5.11 (s, 1H,=C*H*), 2.60 (s, 3H, S–CH_3), 2.27 (s, 3H, C–CH_3), 2.12 (s, 3H, C–CH_3).

7: Claret red, 206, 45. Anal. Calcd for $C_{15}H_{17}N_3O_3SNi$ (378.07 g/M): C, 47.65; H, 4.53; N 11.11; S, 8.48. Found (%): C, 47.35; H, 4.35; N, 11.08; S, 8.30. UV–vis: 251 (5.0), 305 (4.7), 359 (4.6), 392 (4.5), 488 (4.3), 556 (3.9). IR: ν(C=N^1) 1620, ν(N^2=C) 1589 ν(N^4=C) 1571. ^{1}H NMR: 7.88 (s, 1H, N^4=C*H*), 6.92 (t, J = 4.89, J = 7.79, 1H, *d*), 6.72 (t, J = 5.85, J = 6.35 1H, *b*), 6.57 (t, J = 7.32, J = 6.83 1H, *c*), 5.18 (s, 1H,=C*H*), 3.76 (s, 3H, OCH_3) 2.61 (s, 3H, S–CH_3), 2.27 (s, 3H, C-CH_3), 2.02 (s, 3H, C–CH_3).

8: Claret red, 231, 55. Anal. Calcd for $C_{14}H_{13}N_3O_2SNiCI_2$ (416.93 g/M): C, 40.33; H, 3.14; N, 10.08; S, 7.69. Found (%): C, 40.00; H, 3.00; N, 10.01; S, 7.50. UV–vis: 251 (4.8), 298 (4.5), 362 (4.4), 416 (4.3), 492 (4.2), 586 (3.8). IR: ν(C=N^1) 1612, ν(N^2=C) 1590, ν(N^4=C) 1575. ^{1}H NMR: 7.86 (s, 1H, N^4=C*H*), 7.46 (s, 1H, *b*), 7.29 (s, 1H, *d*), 5.23 (s, 1H,=C*H*), 2.61 (s, 3H, S–CH_3), 2.28 (s, 3H, C–CH_3), 2.13 (s, 3H, C–CH_3).

3. Results and discussion

3.1. *Synthesis and some physical properties*

Fine crystals of acetylacetone S-methyl-thiosemicarbazone are soluble in ethanol and chloroform. The template reactions of the thiosemicarbazone with substituted salicylaldehydes in the presence of iron(III) or nickel(II) chloride salts give the chelate complexes, [Fe(L)Cl] and [Ni(L)] (figure 1). The bright black iron and claret red nickel complexes are needle crystals, all soluble in alcohol and chloroform.

3.2. *Spectroscopic data*

Absorption spectra of acetylacetone S-methylthiosemicarbazone in $CHCl_3$ shows three bands at 240, 255, and 358 nm, attributting to $\pi \rightarrow \pi^*$ and $n \rightarrow \pi^*$ transitions corresponding to azomethine and thioamide groups. Intramolecular transitions of the complexes were

observed at 235–240 and 285–298 nm for **1–4** and 240–251, 288–305, and 356–362 nm for **5–8**. Broad bands between 285 and 362 are assigned to $n \rightarrow \pi^*$ transitions on the thiosemicarbazone backbone of the complex structures [28, 29]. Absorptions of the iron(III) complexes, **1–4**, have two main bands in the 418–429 and 529–569 cm^{-1} regions assigned to LM-CT transitions. The electronic spectra of **1–4** did not give information about the expected square-pyramidal structure of the five-coordinate iron(III) because of quite low intensities of d–d transitions. The spectra of the nickel(II) complexes **5–8** display three bands at 392–416, 474–492, and 546–586 nm attributting to $^1A_{1g} \rightarrow {}^1B_{2g}$, $^1A_{1g} \rightarrow {}^1A_{2g}$, and $^1A_{1g} \rightarrow {}^1E_g$ transitions, respectively [28, 30]. The appearances of these bands are consistent with diamagnetic nature of **5–8** and so square-planar geometry around nickel(II).

The infrared spectra of acetylacetone S-methylthiosemicarbazone clearly showed the stretching vibrations of OH, NH_2, $C=N^1$ groups. The $\delta(NH_2)$ and $\nu(C=N)$ bands between 1637 and 1539 cm^{-1} cannot be clearly analyzed as a consequence of the tautomerism represented with $N^2=C(SR)–N^4H_2 \longleftrightarrow N^2H–C(SR)=N^4H$. However, the observation is that the $\nu(OH)$ and $\nu(NH_2)$ bands are absent due to condensation of thioamide nitrogen and aldehyde. After the metal directed condensation, a new azomethine band, $N^4=C$, was at 1581–1571 cm^{-1} as a result of the formation of the N_2O_2 chelate. Thus, the new conjugated backbone of thiosemicarbazone ligand includes three imine bonds which are $C=N^1$, $N^2=C$, and $N^4=C$. It is difficult to distinguish these imine vibrations, but shifting of C=N bands to lower wavenumber by 5–20 cm^{-1} in the metal complexes is in comparison to the S-methylthiosemicarbazone [31].

The formation of the nickel(II) complexes, **5–8**, can also be checked by NMR spectra. Proton signals of phenolic OH and NH_2 disappear due to the complexation. A new proton singlet, equivalent to one proton, indicates formation of $N^4=CH$ and completion of template condensation. ^1H NMR spectra of **5–8** showed expected chemical shifts for the aromatic, azomethine, and S-methyl protons.

Mass spectra provided supporting evidence for the structures of the iron complexes. Some peaks, 375.2 $[M - Cl]^+$ and 376.0 $[M - Cl + H]$ for **3**, and 415.8 $[M - Cl + H]$ and 402.4 $[M–SCH_3]$ for **4** indicated that chlorine and SCH_3 are lost first, as expected.

3.3. *Crystallography*

The basic crystal data and structure refinement parameters for **3** and **7** are shown in table 1 and selected bond distances and angles are presented in table 2.

The template condensation of the S-methylthiosemicarbazone and aldehyde gives a N_2O_2 chelating thiosemicarbazidato ligand (figures 2 and 3). The iron complex **3** has a square-pyramidal geometry with O1, O2, N1, and N3 of the tetradentate thiosemicarbazone moiety, and chloride in the apical position. The chelate complex has three metallo-rings, one five-membered FeN3C and two six-membered FeNC3O, which are not coplanar. The Fe–O1 and Fe–O2 bonds are relatively short in comparison with Fe–N1 and Fe–N3, therefore, the five- and six-membered chelate rings are not regular (table 2). Also, the angles of the coordination bond axes, O1–Fe1–N3 (146.3°) and O2–Fe1–N1 (147.9°), indicate bending of square-planar base in the opposite direction of chloride (Cl1). Iron is above this deformed square base and compared to the other coordination bonds of the molecule, chloride is weakly bonded to iron as evidenced by the 2.236 Å bond length.

The chloride is closer to N1 and N3 compared to O1 and O2 in other edges of pyramid base and results in the square-pyramid distortion in the three-axis direction.

Table 1. Summary of crystal and refinement data for **3** and **7**.

	3	**7**
Empirical formula	$C_{15}H_{17}ClFeN_3O_3S$	$C_{15}H_{17}N_3NiO_3S$
Crystal color, habit	Black, platelet	Red, platelet
Formula weight	410.68	378.08
Temperature (K)	293.1	293.1
Wavelength (Å)	0.7107	0.7107
Crystal system	Triclinic	Triclinic
Space group	*P-1*	*P-1*
Cell dimensions (Å, °)	a = 8.458(6)	a = 7.729(11)
	b = 8.605(5)	b = 10.097(13)
	c = 13.487(2)	c = 10.810(10)
	α = 79.31(3)	α = 99.688(4)
	β = 88.58(3)	β = 97.953(4)
	γ = 67.24(2)	γ = 100.717(7)
Cell volume	888.5(2)	804.6(2)
Cell formula units (Z)	2	2
Density (calculated)	1.53	1.561
Absorption coefficient	1.133	1.353
F (0 0 0)	422	392
h, k, l ranges	−9/10, −10/10, −16/16	−9/8, −12/12, −12/12
Reflections collected	42,918	34,870
Independent reflections	3138 [R_{int} = 0.064]	2645 [R_{int} = 0.038]
Data/restraints/parameters	3138/0/234	2645/0/231
Goodness of fit indicator	1.241	0.954
Final R indices [$I > 2\sigma(I)$]	R = 0.079, Rw = 0.066	R = 0.045, Rw = 0.052
Largest diff. peak and hole (e Å^{-3})	0.44 and −0.73	0.29 and −0.30

Table 2. Selected bond lengths (Å) and angles (°) for **3** and **7**.

Bond	Distance	Bond	Distance
Fe1–O1	1.905(4)	Ni1–O1	1.840(2)
Fe1–O2	1.887(3)	Ni1–O2	1.841(2)
Fe1–N1	2.047(4)	Ni1–N1	1.845(3)
Fe1–N3	2.086(3)	Ni1–N3	1.833(2)
Fe1–Cl1	2.236(2)		
Bond	**Angle**	**Bond**	**Angle**
O1–Fe1–O2	95.0(1)	O1–Ni1–O2	86.07(9)
O1–Fe1–N1	87.2(1)	O1–Ni1–N1	177.77(8)
O2–Fe1–N3	86.3(1)	O2–Ni1–N3	178.5(1)
N3–Fe1–N1	74.8(1)	N3–Ni1–N1	83.8(1)
O2–Fe1–N1	147.9(2)	O2–Ni1–N1	95.01(9)
O1–Fe1–N3	146.3(2)	O1–Ni1–N3	95.2(1)
Cl1–Fe1–O1	110.5(1)	Cl1–Fe1–O2	107.0(1)
Cl1–Fe1–N1	102.1(1)	Cl1–Fe1–N3	101.1(1)

Four-coordinate nickel(II) connects with thiosemicarbazone through O1, O2, N1, and N3 forming a square-planar environment around nickel(II). Nickel coordination bonds are approximately the same length and distortions in diagonal axes of the square-plane are negligible considering the angle values of O1–Ni1–N1 (177.77°) and O2–Ni1–N2 (178.5°). Therefore, two five-membered NiN3C and two six-membered NiONC3 chelate rings in the structure are almost coplanar. Given the asymmetric structure of **7** (because of different moieties bonded to N1 and N4), this square-plane is fairly uniform.

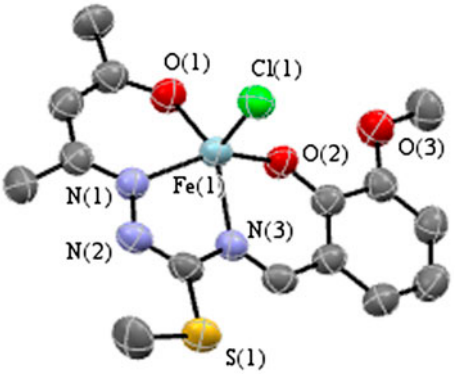

Figure 2. ORTEP diagram of **3** excluding hydrogens.

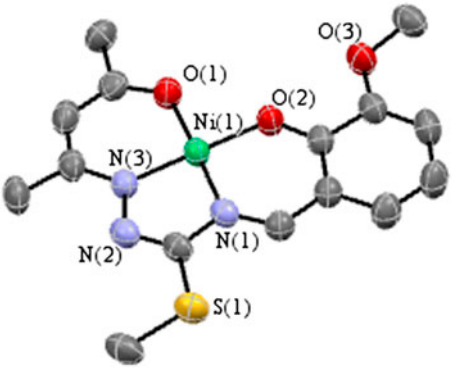

Figure 3. ORTEP diagram of **7** excluding hydrogens.

The square-planar base of **3** is approximately parallel, but benzene rings of adjacent molecules are located so as to be on opposing sides. A similar arrangement was also observed in the crystal of **7**. There are no hydrogen bonds or significant intermolecular interactions in the crystal structures of **3** and **7**.

3.4. *Electrochemistry*

Electrochemical analysis of the iron(III) and nickel(II) complexes were studied using CV and SWV measurements in DCM and DMSO containing TBAP as supporting electrolyte on a Pt working electrode. Table 3, lists the assignments of the redox couples and the electrochemical parameters, which included the half-wave peak potentials ($E_{1/2}$), anodic to cathodic peak potential separation (ΔE_p), and ratio of the anodic to cathodic peak currents (I_{pa}/I_{pc}). All complexes, **1–8**, gave an irreversible one-electron oxidation and an irreversible one-electron reduction within the potential window of the electrolyte systems. The one-electron nature of these processes has been established by comparing their peak current height with that of the standard ferrocene/ferrocenium couple under identical experimental

Table 3. Voltammetric data of the complexes.

Complexes	Peak parameters	Redox processes		
		L/L^+	Metal reduction	L/L^-
1 (in DCM)	[a]$E_{1/2}$ 0	1.10	−0.22	−1.40 (−1.50[d])
	[b]ΔE_p (mV)	90	70	–
	[c]I_{pa}/I_{pc}	0.38	0.92	–
2 (in DCM)	[a]$E_{1/2}$ 0	1.24	−0.20	−1.28 (−1.50[d])
	[b]ΔE_p (mV)	100	150	–
	[c]I_{pa}/I_{pc}	0.41	0.95	–
3 (in DCM)	[a]$E_{1/2}$ 0	1.10	−0.31	−1.58
	[b]ΔE_p (mV)	90	70	115
	[c]I_{pa}/I_{pc}	0.38	0.92	0.54
4 (in DCM)	[a]$E_{1/2}$	1.30	−0.12	−1.18
	[b]ΔE_p (mV)	100	65	120
	[c]I_{pa}/I_{pc}	0.40	0.94	0.34
4 (in DMSO)	[a]$E_{1/2}$	0.94	−0.15	−1.32
	[b]ΔE_p (mV)	130	58	68
	[c]I_{pa}/I_{pc}	0.65	0.98	0.34
5 (in DCM)	[a]$E_{1/2}$	1.17	–	−1.38
	[b]ΔE_p (mV)	72	–	80
	[c]I_{pa}/I_{pc}	0.55	–	0.51
6 (in DCM)	[a]$E_{1/2}$	1.18	–	−1.10
	[b]ΔE_p (mV)	76	–	75
	[c]I_{pa}/I_{pc}	0.45	–	0.32
7 (in DCM)	[a]$E_{1/2}$	1.12	–	−1.42
	[b]ΔE_p (mV)	79	–	77
	[c]I_{pa}/I_{pc}	0.62	–	0.56
8 (in DCM)	[a]$E_{1/2}$	1.22	–	−1.00
	[b]ΔE_p (mV)	74	–	70
	[c]I_{pa}/I_{pc}	0.41	–	0.35
8 (in DMSO)	[a]$E_{1/2}$	0.82	–	−0.98
	[b]ΔE_p (mV)	80	–	60
	[c]I_{pa}/I_{pc}	0.48	–	0.42

[a]$E_{1/2} = (E_{pa} + E_{pc})/2$ at 0.100 V s^{-1}.
[b]$\Delta E_p = |E_{pc} + E_{pa}|$.
[c]I_{pa}/I_{pc} for reduction, I_{pc}/I_{pa} for oxidation processes at 0.100 V s^{-1} scan rate.
[d]$E_{1/2}$ values for the third reduction reactions.

conditions. CPC analysis of the complexes also indicated one-electron transfer features of the redox processes [32].

The nickel(II) complexes showed similar voltammetric responses, therefore CV and SWV responses of **8** are given in figure 4, as a representative of the nickel complexes. Complex **8** gives a one-electron irreversible reduction at −1.00 V and a one-electron irreversible oxidation process at 1.22 V in TBAP/DCM electrolyte system. Both reduction and oxidation could be assigned to ligand based processes. It is reported that these ligands gave a one-electron irreversible oxidation and one-electron irreversible reduction processes at the end of the DCM or DMSO/TBAP electrolyte windows and coordination of the ligands to metal ion did not significantly affect the redox potential of ligands. The redox responses of nickel complexes are consistent with similar ones in the literature [33–35]. For example, H. Bingol and co-workers reported two oxidation processes after 1.0 V and a reduction peak at −0.45 V for a nickel thiosemicarbazone [36]. They assigned these processes to the electron transfer reactions of imine and thioamide group of thiosemicarbazone ligands. In our previous papers, we reported similar redox responses for various N_2O_2 or N_2S_2 type complexes [43–47]. This voltammetric behavior shows that reduced complexes give a chemical reaction and the products of this chemical reaction give the CP_1 wave.

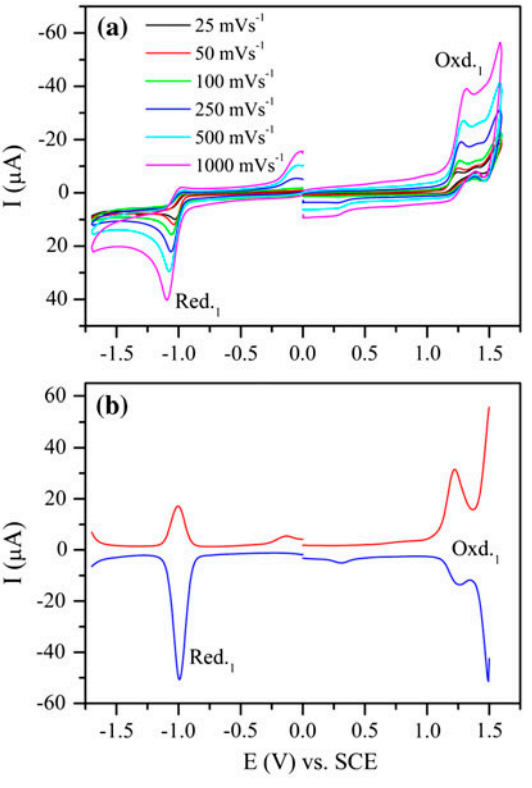

Figure 4. (a) CVs of **8** recorded at various scan rates in TBAP/DCM electrolyte system on Pt working electrode. (b) SWV of **8** recorded with the SWV parameters: pulse size = 100 mV; pulse width = 5 mV; frequency: 25 Hz.

Redox responses of other nickel(II) complexes were also determined to indicate the effect of the substituents to the electrochemical responses of the complexes. The only difference between the redox responses of the complexes, is shifting of the redox processes due to the different electron releasing abilities of the substituents. While **8** (3,5-dichloro substituted) reduced at the most positive potential, **7** (3-methoxy substituted) reduced at the most negative potential among all nickel complexes.

Iron(III) complexes give completely different voltammetric responses than those of nickel (II) complexes. While nickel(II) complexes only give a ligand based reduction and a ligand based oxidation, iron(III) complexes give a reversible metal-based reduction in addition to the ligand based reduction and oxidation reactions [48, 49]. Figure 5, represents CV and SWV responses of **4** in TBAP/DCM electrolyte system. Complex **4** gives a reversible reduction couple $Red._1$ at −0.12 V and an irreversible reduction wave $Red._2$ at −1.18 V during the cathodic potential scans and an irreversible oxidation wave $Oxd._1$ at 1.30 V. ΔE_p of the Fe^{III}/Fe^{II} couple is in a reversible range especially at very slow scan rates and unity of the I_{pa}/I_{pc} ratios and linearity of I_p *versus* $v^{1/2}$ changes, indicating the reversible character of this redox process; $Red._2$ and $Oxd._1$ processes are electrochemically and chemically irreversible.

Electrochemical analysis of **4** is also performed in TBAP/DMSO electrolyte system to illustrate the solvent effects. Figure 6 shows similar CV and SWV responses with slight

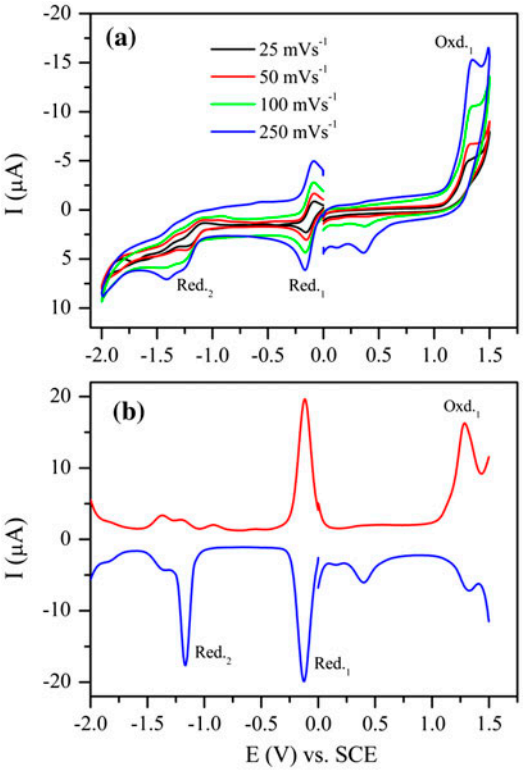

Figure 5. (a) CVs of **4** recorded at various scan rates in TBAP/DCM electrolyte system on Pt working electrode. (b) SWV of **4** recorded with the SWV parameters: pulse size = 100 mV; pulse width = 5 mV; frequency: 25 Hz.

difference in peak potentials, reversibility of the peaks, and chemical stability of the electrogenerated species. While reduction processes of the complex are electrochemically more reversible in DMSO, electrochemical reversibility of the complex is worse in DMSO with respect to DCM. As shown in figure 6, due to the presence of a chemical reaction following $Red._2$ process, a wave $CP._1$ assigned to oxidation of chemical products is observed at −0.52 V.

The electrochemical behaviors of iron complexes are in agreement with similar complexes reported [37–39]. Iron thiosemicarbazone derivatives generally have Fe(III)/Fe(II) based reduction processes between 0 and −0.5 V, depending on the substituents of thiosemicarbazone ligands [37, 38]. For example, S.K. Kar reported reversible Fe(III)/Fe(II) reduction couples at 0 V. They also showed that the peak potential of this wave shifted to −0.31 V with substitution of the complexes with electron-releasing ligands. Similarly, Beraldo *et al*. presented metal-based redox activity of an iron thiosemicarbazone derivative [38], indicating that Fe(III) reduced to Fe(II) at −0.20 V. Arion *et al.* indicated Fe(III)/Fe(II) based activities of 14 different iron thiosemicarbazone derivatives which gave reversible metal-based reduction between 0 and 0.30 V *versus* NHE in 0.20 M [n-Bu_4 N][BF_4]/CH_3CN [39].

Reversible reduction processes of **1–4** indicate their potential in various technologies, especially electrocatalytic and electrochemical sensor applications. Minimum requirement of these applications is the existence of at least one reversible metal-based electron transfer

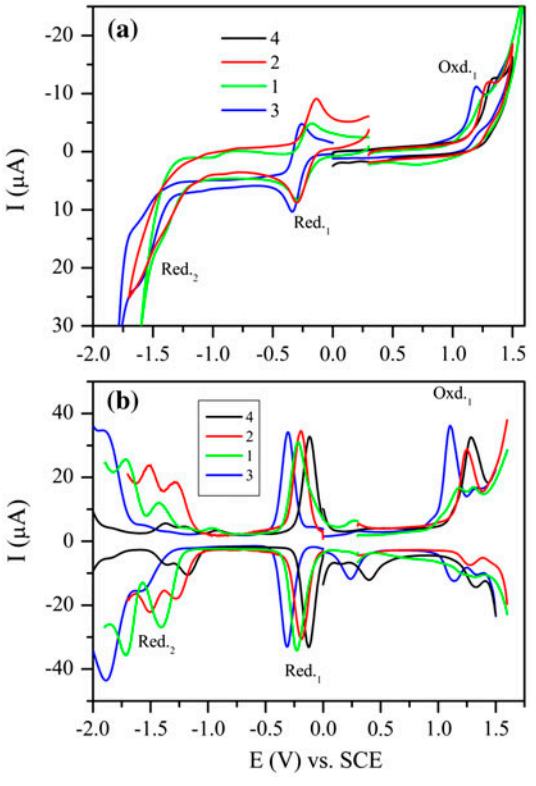

Figure 6. (a) CVs of iron(III) complexes (**1**–**4**) recorded at 0.10 V s^{-1} scan rate in TBAP/DCM electrolyte system on Pt working electrode. (b) SWV of **1**–**4** recorded with the SWV parameters: pulse size = 100 mV; pulse width = 5 mV; frequency: 25 Hz.

reaction at small potentials. Shifting of the redox processes with different substituents on the ligands indicate that redox processes of these complexes could be arranged for the desired applications. Thiosemicarbazone derivatives were also used in antimicrobial applications [38, 40–42]. For these applications, the complex should have a reversible redox process at around 0 V and this process should be changed as a result of the interaction with the target species.

CV and SWV responses indicated substituent effects to the electrochemical properties of the iron(III) complexes, due to differences of substituents by the Red.1 couples of the complexes (see table 3). While **4** (3,5-dichloro substituted) gives $Red._1$ couple at −0.12 V in TBAP/DCM, changing the substituents shifts this couple and **3** (3-methoxy substituted) gives $Red._1$ couple at the most negative potential (−0.31 V).

4. Conclusion

Template condensation of S-alkyl thiosemicarbazones derived from various salicylaldehydes and benzophenones have been reported [15–17, 22, 48, 50, 51]. Structural analysis of the iron(III) complexes (**1–4**) obtained from acetylacetone-S-methyl-thiosemicarbazone

was reported for the first time. New nickel(II) complexes (**5–8**) of the same thiosemicarbazone ligands were also reported. X-ray diffraction analysis of the methoxy substituted nickel and iron complexes confirmed the N_2O_2 chelate structures of **1–8**.

Complexes **1–8** are promising for cytotoxic potential like analog N^1,N^4-diarylidene-thiosemicarbazidato iron(III) and nickel(II) complexes [14, 22]. Some electrochemical parameters of the complexes were determined to understand the behavior of these chelate complexes in biological systems. CV and SWV analysis indicates that while all complexes give irreversible ligand based oxidation and reduction reactions, iron(III) complexes (**1–4**) give reversible Fe^{III}/Fe^{II} based reduction reactions at 0 V. Observation of reversible metal-based redox processes at small potentials increases the potential in various electrochemical technologies such as: electrocatalytic, electrosensing, and microbial applications. Altering the redox processes with different substituents indicates possibilities of arranging electrochemical behaviors for desired applications.

Supplementary material

CCDC 976049 and 976048 contain the supplementary crystallographic data for **3** (C15H17Cl1Fe1N3O3S1) and **7** (C15H17N3Ni1O3S1). These data can be obtained free of charge via http://www.ccdc.cam.ac.uk/conts/retrieving.html, or from the Cambridge Crystallographic Data Center, 12 Union Road, Cambridge CB2 1EZ, UK; Fax: (+44) 1223-336-033; or E-mail: deposit@ccdc.cam.ac.uk.

Funding

The present work was supported by Turkish Academy of Sciences (TUBA) and Research Fund of Istanbul University [Grant Number Project No. 32050].

References

[1] H. Beraldo, D. Gambino. *Mini-Rev. Med. Chem.*, **4**, 31 (2004).
[2] P. Mantegazza, R. Tommasini. *Farmaco*, **6**, 264 (1951).
[3] S. Padhye, Z. Afrasiabi, E. Sinn, J. Fok, K. Mehta, N. Rath. *Inorg. Chem.*, **44**, 1154 (2005).
[4] Z. Afrasiabi, E. Sinn, W. Lin, Y. Ma, C. Campana, S. Padhye. *J. Inorg. Biochem.*, **99**, 1526 (2005).
[5] J. Patole, S. Padhye, M.S. Moodbidri, N. Shirsat. *Eur. J. Med. Chem.*, **40**, 1052 (2005).
[6] M.C. Rodríguez-Argüelles, E.C. López-Silva, J. Sanmartín, A. Bacchi, C. Pelizzi, F. Zani. *Inorg. Chim. Acta*, **357**, 2543 (2004).
[7] V.I. Prisakar, V.I. Tsapkov, S.A. Buracheeva, M.S. Byrke, A.P. Gulya. *Pharm. Chem.*, **39**, 313 (2005).
[8] A. De Logu, M. Saddi, V. Onnis, C. Sanna, C. Congiu, R. Borgna, M.T. Cocco. *Int. J. Antimicrob. Agents*, **26**, 28 (2005).
[9] T. Varadinova, D. Kovala-Demertzi, M. Rupelieva, M. Demertzis, P. Genova. *Acta Virol.*, **45**, 87 (2001).
[10] P. Genova, T. Varadinova, A.I. Matesanz, D. Marinova, P. Souza. *Toxicol. Appl. Pharmacol.*, **197**, 107 (2004).
[11] T.R. Bal, B. Anand, P. Yogeeswari, D. Sriram. *Bioorg. Med. Chem. Lett.*, **15**, 4451 (2005).
[12] M. Karatepe, F. Karatas. *Cell Biochem. Funct.*, **24**, 547 (2006).
[13] D.X. West, A.E. Liberta. *Coord. Chem. Rev.*, **123**, 49 (1993).
[14] T. Bal Demirci, B. Atasever, Z. Solakoğlu, S. Erdem-Kuruca, B. Ülküseven. *Eur. J. Med. Chem.*, **42**, 161 (2007).
[15] N.V. Gerbeleu, V.B. Arion, J. Burgess. *Template Synthesis of Macrocyclic Compounds*, Wiley-VCH, Weinheim (1999).
[16] J. Gradinaru, Y.A. Simonov, V.B. Arion, P.N. Bourosh, M.A. Popovici, V.K. Bel'skii, N.V. Gerbeleu. *Inorg. Chim. Acta*, **30**, 313 (2001).
[17] A. Forni, J. Gradinaru, V. Druta, S. Zecchin, S. Quici, N. Gerbeleu. *Inorg. Chim. Acta*, **338**, 169 (2002).

[18] J. Gradinaru, A. Forni, N. Buza, N. Gerbeleu. *Inorg. Chim. Acta*, **357**, 875 (2004).
[19] V.M. Leovac, V. Divjaković, V.I. Češljević, P. Engel. *Polyhedron*, **6**, 1901 (1987).
[20] V.M. Leovac, V.I. Cesljevic, S.M. Nesic. *Z. Anorg. Allg. Chem.*, **592**, 217 (1991).
[21] J. Gradinaru, A. Forni, Y. Simonov, M. Popovici, S. Zecchin, M. Gdaniec, D.E. Fenton. *Inorg. Chim. Acta*, **357**, 2728 (2004).
[22] B. Atasever, B. Ülküseven, T. Bal-Demirci, S. Erdem-Kuruca, Z. Solakoğlu. *Invest. New Drugs*, **28**, 421 (2010).
[23] A. Altomare, G. Cascarano, C. Giacovazzo, A. Guagliardi, M. Burla, G. Polidori, M. Camalli. *J. Appl. Cryst.*, **27**, 435 (1994).
[24] Crystal Structure 3.5.1. *Crystal Structure Analysis Package*, Rigaku and Rigaku/MSC, 9009 New Trails Dr., The Woodlands, TX, 2000–2003.
[25] D.J. Watkin, C.K. Prout, J.R. Carruthers, P.W. Betteridge. *Crystals, Issue 10*, Chemical Crystallography Laboratory, Oxford (1996).
[26] C. Yamazaki. *Can. J. Chem.*, **53**, 610 (1975).
[27] T. Bal, B. Ülküseven. *Transition Met. Chem.*, **29**, 880 (2004).
[28] L.M. Fostiak, I. García, J.K. Swearingen, E. Bermejo, A. Castiñeiras, D.X. West. *Polyhedron*, **22**, 83 (2003).
[29] H. Beraldo, L.P. Boyd, D.X. West. *Transition Met. Chem.*, **23**, 67 (1998).
[30] A.B.P. Lever. *Inorganic Electronic Spectroscopy*, 2nd Edn, Elsevier, Amsterdam (1984).
[31] V.B. Arion, V.C. Kravtsov, R. Goddard, E. Bill, J.I. Gradinaru, N.V. Gerbeleu, V. Levitschi, H. Vezin, Y.A. Simonov, J. Lipkowski, V.K. Bel'skii. *Inorg. Chim. Acta*, **317**, 33 (2001).
[32] W.R.H. Peter Kissinger. *Laboratory Techniques in Electroanalytical Chemistry*, 2nd Edn, Marcel Dekker, New York (1996).
[33] Y. Harek, L. Larabi, L. Boukli, F. Kadri, N. Benali-Cherif, M. Mostafa. *Transition Met. Chem.*, **30**, 121 (2005).
[34] N.V. Kulkarni, M.P. Sathisha, S. Budagumpi, G.S. Kurdekar, V.K. Revankar. *J. Coord. Chem.*, **63**, 1451 (2010).
[35] R. Prabhakaran, R. Sivasamy, J. Angayarkanni, R. Huang, P. Kalaivani, R. Karvembu, F. Dallemer, K. Natarajan. *Inorg. Chim. Acta*, **374**, 647 (2011).
[36] H. Bingol, A. Coskun, E.G. Akgemci, B. Kaya, T. Atalay. *Chin. J. Chem.*, **25**, 307 (2007).
[37] S. Pal, A.K. Barik, P. Aich, S.M. Peng, G.H. Lee, S.K. Kar. *Struct. Chem.*, **18**, 149 (2007).
[38] R.F.F. Costa, A.P. Rebolledo, T. Matencio, H.D.R. Calado, J.D. Ardisson, M.E. Cortés, B.L. Rodrigues, H. Beraldo. *J. Coord. Chem.*, **58**, 1307 (2005).
[39] C.R. Kowol, E. Reisner, I. Chiorescu, V.B. Arion, M. Galanski, D.V. Deubel, B.K. Keppler. *Inorg. Chem.*, **47**, 11032 (2008).
[40] A. Mohsen, M.E. Omar, N.S. Habib. *Pharmazie*, **33**, 81 (1978).
[41] A. Omar, I.M. Labouta, M.G. Kasem, J. Bourdais. *J. Pharm. Sci.*, **72**, 1226 (1983).
[42] E. Melton, C. Thompson, K. Mansur, E.C. Lisic. 245th ACS National Meeting & Exposition, New Orleans, LA, 7–11 April (2013), CHED-816.
[43] S. Duman, I. Kizilcikli, A. Koca, M. Akkurt, B. Ülküseven. *Polyhedron*, **29**, 2924 (2010).
[44] M. Şahin, A. Koca, N. Özdemir, M. Dinçer, O. Büyükgüngör, T. Bal-Demirci, B. Ülküseven. *Dalton Trans.*, **39**, 10228 (2010).
[45] M. Kandaz, O. Katmer, A. Koca. *Transition Met. Chem.*, **31**, 889 (2006).
[46] A. Erçağ, M. Şahin, A. Koca, E. Bozkurt. *J. Coord. Chem.*, **66**, 1635 (2013).
[47] M.N. Yaraşir, M. Kandaz, A. Akyıldız, K. Karadeniz, F. Dumludağ, A. Koca. *Monatsch. Chem.*, **144**, 951 (2013).
[48] Y. Kurt, A. Koca, M. Akkurt, B. Ülküseven. *Inorg. Chim Acta*, **388**, 148 (2012).
[49] M.T. Basha, J.D. Chartres, N. Pantarat, M.A. Ali, A.H. Mirza, D.S. Kalinowski, D.R. Richardson, P.V. Bernhardt. *Dalton Trans.*, **41**, 6536 (2012).
[50] K. Drabent, J.A. Wolny, M.F. Rudolf, P.J. Chmielewski. *Polyhedron*, **11**, 271 (1992).
[51] M. Ahmadi, J.T. Mague, A. Akbari, R. Takjoo. *Polyhedron*, **42**, 128 (2012).